

ANALYSIS OF THE THERMAL MECHANISM AND TEMPORAL AND SPATIAL EVOLUTION OF THE THERMAL FIELD OF DEEP SANDSTONE UNDER MICROWAVES

by

**Ben-Gao YANG^{a,b}, Ming-Zhong GAO^{a,b*}, Jing XIE^{a,b},
Jun-Jun LIU^{a,b}, and Yi-Ting LIU^{a,b}**

^a State Key Laboratory of Hydraulics and Mountain River Engineering,
College of Water Resource and Hydropower, Sichuan University, Chengdu, Sichuan, China

^b Guangdong Provincial Key Laboratory of Deep Earth Sciences and
Geothermal Energy Exploitation and Utilization,
Institute of Deep Earth Sciences and Green Energy,
College of Civil and Transportation Engineering, Shenzhen University, Shenzhen, Guangdong, China

Original scientific paper
<https://doi.org/10.2298/TSCI2006877Y>

In the practice of the deep engineering, it is expected to improve engineering efficiency by introducing the microwave energy. Therefore, based on 1050 m deep sandstone, the heating characteristics of sandstone and its constituent minerals in the microwave field are comprehensively explored through experiments and numerical simulations. In the paper, the asynchronism of the temperature rise in different areas of the sandstone depends on the local characteristics of dielectric loss and maximum heat storage capacity. With increase of the temperature, the evaporation of the water leads to the decrease of the dielectric properties, the increase in the constant-pressure heat capacity and the increase in the heat dissipation coefficient, which suppresses the temperature growth trend. The temperature rise of the amplitude of the material is lower than that expected from the microwave power. The maximum temperature of dolomite, feldspar and quartz under the power of 2000 W is 1.86, 1.71, and 1.63 times that of the power of 1000 W, respectively. It is necessary to select the reasonable microwave power to maximize the engineering efficiency. The results are expected to provide the theoretical and technical supports for the electromagnetic heat generation in deep engineering.

Key words: *deep, microwave, sandstone, mineral, heating*

Introduction

Since the start of the 21st century, with the population expanding and resource consumption surging, shallow space and resources can no longer meet development needs. It is essential to pursue deep-Earth exploration [1, 2]. However, in the development of deep areas and the exploitation of deep resources, it is inevitable to face the problems of a large amount of hard rock fragmentation, high in situ stress and complex resource occurrence conditions. Therefore, microwaves have been gradually introduced into the field of geotechnical, mining and metallurgical engineering due to their advantages of rapid heat production and selective

* Corresponding author, e-mail: gmzh@scu.edu.cn

heating. Replacing part or all of the mechanical energy with microwave energy can solve such engineering problems and improve engineering efficiency.

The heat generation effect of microwaves was first applied in the field of food heating, in the form of microwave ovens. In the mid-1970's, due to the shortage of international oil and natural gas and the rising cost of energy, extensive research was conducted on the application of microwave energy [3]. The microwave heating technology has been widely used in environmental engineering [4, 5], the petrochemical industry [6], food and medicine [7], and other fields. In the field of geotechnical, mining and metallurgy, the microwaves have an enormous market application prospect because of their advantages of fast heat production and selective heating in [8]. The bioleaching and dissolution behavior of low-grade complex sulfide ore after microwave treatment by using the heat generation effect of microwaves was studied in [9]. The microwave irradiation method to extract double refractory gold ore and concluded that microwave energy can be used as an alternative energy source to process ore in some unit operations [10]. In the field of geotechnical engineering, the microwave sensitivity of many kinds of rocks and quantitatively characterized the degradation effect of microwaves on rocks by measuring the temperature rise, Brazilian splitting strength, uniaxial compressive strength and fracture toughness were considered in [11]. The micro weakening mechanism of rock under microwave irradiation by means of mechanical tests and micro scanning was investigated in [12], and the test results showed that the microwave could potentially solve gas outbursts in deep engineering [13, 14] because of that the microwave irradiation could crack rocks. They also carried out experiments at the engineering scale and confirmed the feasibility of applying microwave energy to engineering practice.

In summary, in the field of mining, metallurgy and geotechnical engineering, scholars have carried out much research on the heat generation effect of microwaves and made some important progress. Most of the current research has focused on changes in the macro and micro characteristics of the dielectric materials before and after the action of the microwave field to analyze the influence of the microwave thermal effect on the macro and micro properties. The research progress mainly involves the damage characteristics of materials caused by microwaves. Therefore, this paper takes 1050 m deep sandstone as the research object, studies the electromagnetic heat generation characteristics of sandstone and its minerals in a microwave field by means of indoor tests and numerical simulations, and explores the heat generation mechanism of deep sandstone in a microwave field.

Test plan

Sample preparation

All sandstone samples are taken from the working face with a burial depth of 1050 m in the Pingdingshan coal mine area, Henan Province, China. Then, they are processed into a cylindrical size of $\varnothing 25 \times 50$ mm. All samples selected in the test are taken from the same rock to reduce the test error. Upon grinding samples into powder, the XRD results show that the sandstone is composed mainly of quartz 58%, feldspar 38.5%, and dolomite 3.5%.

Test method

We pasted a PT-100 platinum resistance temperature sensor on the sandstone sample and mineral sample, as shown in fig. 1. After the glue had solidified, the temperature rise characteristic test of the sample was carried out. We placed the sample in the microwave cavity and led a wire out through a cut-off waveguide hole to connect with a paperless recorder, which recorded the data every two seconds. In addition, to eliminate the influence of glue, a pre-ex-

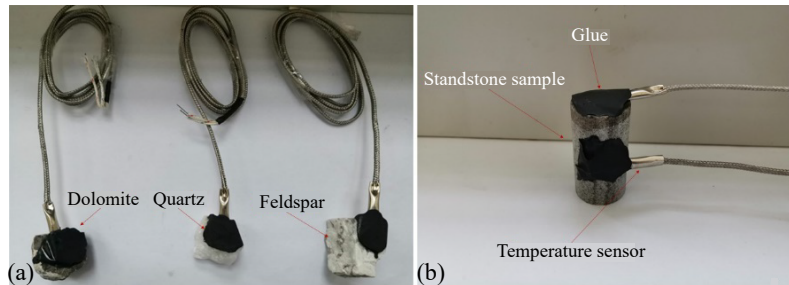


Figure 1. (a) Mineral sample and (b) sandstone sample

periment was carried out in the microwave cavity with a glue configuration sensor alone under 1000 W microwave power. The results indicated that the temperature of the glue in the microwave field would not significantly change the results.

Temperature rise characteristics of sandstone and its minerals under microwave energy

Temperature rise characteristics of sandstone under different microwave powers

The microwave field power is one of the important key parameters that affect the heat production of dielectric materials. To explore the influence of power on the heat production performance of materials, temperature rise tests of sandstone are performed at 200, 600, and 1000 W. A time of 120 seconds before microwave application is selected to analyze the temporal and spatial evolution characteristics of the sandstone temperature rise in the microwave field.

Figure 2 indicates that as the microwave power increases, the temperature of the dielectric material increases to a certain extent. Moreover, the temperature rise in different regions of the dielectric material in the microwave field is asynchronous and varies under different powers. As shown in fig. 2(a) and 2(b), when the power is 200 W or 600 W, the temperature of the sandstone shows a rapid upward trend, indicating that within 120 seconds of irradiation, the two parts of the monitored sandstone have not reached their maximum heat storage capacity and can continue to absorb microwave energy to generate heat. Due to the difference in the absorption ability of each area, the temperature gradient is continuously amplified. As shown in fig. 2(c), when the power is 1000 W, the temperature in the first monitoring point area has entered a stable state and essentially no longer increases, indicating that the area has reached its maximum heat storage capacity. The temperature in the other area is still growing rapidly and has not yet reached its maximum heat storage capacity. Therefore, the temperature gradient between the two areas shows a decreasing trend.

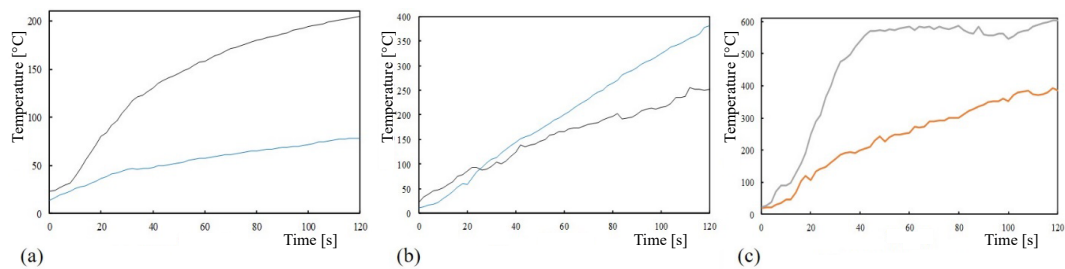


Figure 2. Temperature rise data monitoring of sandstone under different powers changes at; (a) 200 W, (b) 600 W, and (c) 1000 W

Heating characteristics of different minerals under microwave energy

To further explore the internal relationship between the heat generation mechanism of rocks in the microwave field and their constituent minerals, temperature rise tests of different minerals in the microwave field under 600 W and 1000 W power were designed and carried out for the main rock-forming minerals of quartz, feldspar and dolomite in sandstone. Figures 3 and 4 show that there are great differences in the heat production of different minerals in the microwave field, and the heat production characteristics are also affected by the microwave power. Figure 3 shows that under 600 W, the thermal performance of dolomite and feldspar is relatively close. In addition, figs. 3 and 4 also show that in the microwave field, the temperature rise rate of the three minerals exhibit a turning point when the temperature exceeds 100 °C, and the temperature rise rate decreases. A possible reason is that water exists in the mineral materials as a polar molecule. Due to the high temperature, the structural water, free water and other water molecules in the materials evaporate, resulting in a decrease in the dielectric properties of the mineral, and the constant-pressure heat capacity of the mineral itself increases with increasing temperature. The heat dissipation of the material increases nonlinearly with increasing temperature. Under the joint action of many factors, the rising temperature trend slows down.

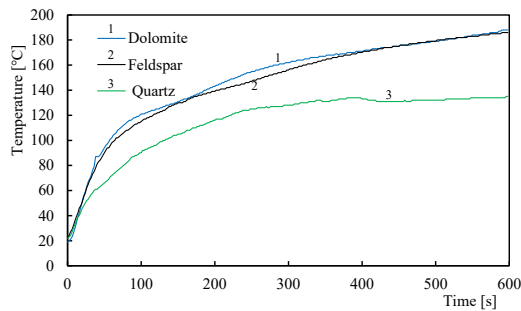


Figure 3. Changes at 600 W

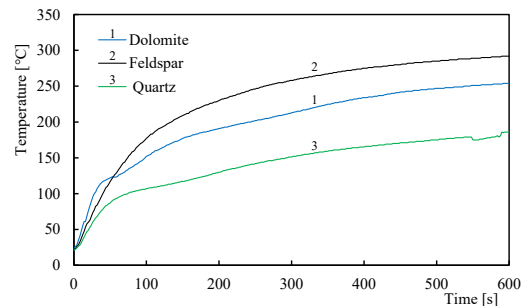


Figure 4. Changes at 1000 W

To further explore the relationship between microwave power and different mineral heat production rates, the temperature scale factor, q , is defined to quantitatively characterize the difference in mineral heat production. This factor reflects the temperature ratio for the same time under different powers, which is given:

$$q = \frac{T_{p1000}}{T_{p600}} \quad (1)$$

where q is the temperature scale factor, T_{p1000} is the mineral surface temperature under the power 1000 W, and T_{p600} is the mineral surface temperature under the power 600 W. When ignoring the influence of the initial ambient temperature on the initial value of the temperature scale factor, it can be seen from fig. 5 that only the heat production of feldspar has a linear relationship with increasing power, while the temperature ratio factors of dolomite and quartz are lower than 1.7.

Thermal sensitivity analysis of sandstone under microwave energy

Three-dimensional, three-phase mineral model construction

The indoor test results reveal that heating in the microwave field is controlled by the microwave power, and the heating is different in different areas. In fact, the dielectric mate-

rial is affected by the electromagnetic field, temperature field and other physical fields in the microwave field, and the internal temperature rise of the dielectric material is also affected by the internal mineral distribution, heat conduction and electric field distribution. To further explore the influence of various factors on the temperature rise of the material, COMSOL is used to establish a 3-D, three-phase mineral model. We analyze the temperature-electric field spatiotemporal evolution of typical points and surfaces. Considering the complexity of the actual material composition, it is impractical to completely simulate the real physical experiment. Therefore, to simplify the model calculation, a 3-D, three-phase model of the microwave field is established for the heat generation of the minerals inside the sandstone and the heat conduction between the minerals in the microwave field, as shown in fig. 6. The model is composed mainly of a microwave feed, a resonant cavity and a 3-D mineral model of quartz-feldspar-dolomite. Microwave feeders and resonators are reconstructed according to the actual geometry. The 3-D mineral model is shown in fig. 7.

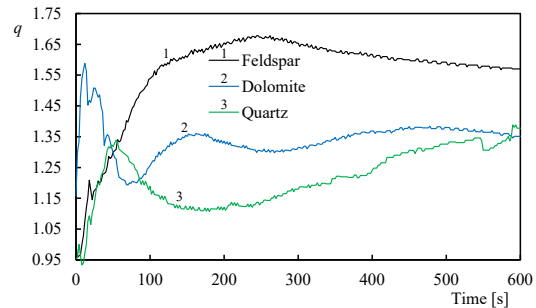


Figure 5. Changes of the temperature scale factor

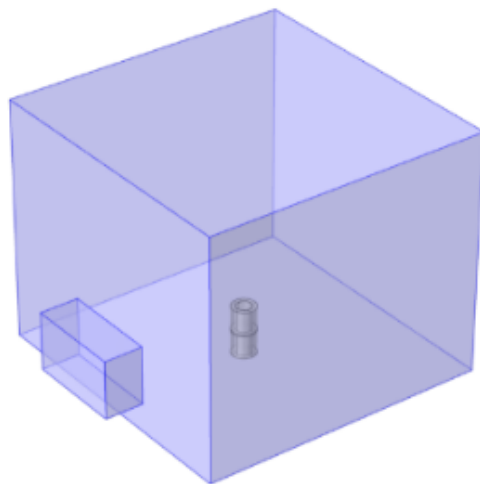


Figure 6. The cavity model

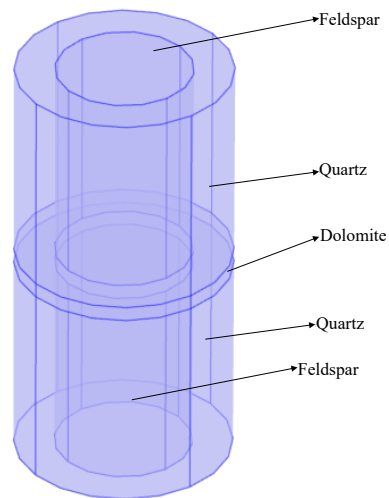
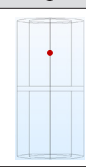



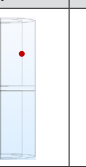
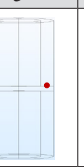
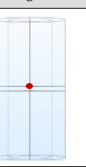
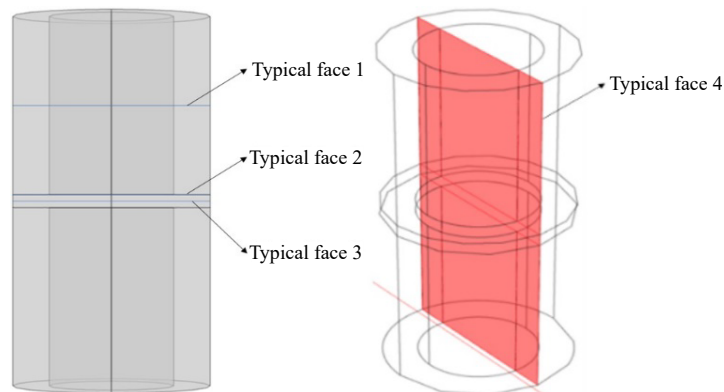


Figure 7. Dielectric material model

In the microwave field, the power and duration of microwaves are the key parameters that affect the heat production of dielectric materials. Therefore, it is necessary to explore the temperature evolution law of the typical points and surfaces within and between minerals under different microwave powers and times. The selected typical monitoring points are shown in tab. 1, including the internal points of each mineral, the two-phase mineral contact points and the three-phase mineral contact points. The typical surface is shown in fig. 8. The material longitudinal profile, the center surface of the upper cylinder, the top surface of the dolomite and the center surface of the dolomite are selected as the typical surface.

Table 1. The monitoring points of the typical minerals

Measurement points	1	2	3	4	5	6	7
Schematics							

**Figure 8. The typical diagram**

Governing equations

The microwave field is an electromagnetic-thermal multi-field coupling process, which consists of two parts: electromagnetic heat generation and solid heat transfer. When using frequency domain and transient methods to solve electromagnetic field problems, the governing equation is the Helmholtz vector equation [15], e. g.:

$$\nabla \times \mu_r^{-1} (\nabla \times \mathbf{E}) - k_0^2 \left(\varepsilon_r - \frac{j\sigma}{\omega \varepsilon_0} \right) \mathbf{E} = 0 \quad (2)$$

where μ_r is the relative permeability, \mathbf{E} – the electric field strength, k_0 – the free space wave velocity, σ – the conductivity, ε_r – the dielectric constant, ω – the angular frequency, and ε_0 – the vacuum dielectric constant. The control equation of electromagnetic heat generation is [16]:

$$Q_e = Q_{rh} + Q_{ml} \quad (3)$$

$$Q_{rh} = \frac{1}{2} \text{Re}(\mathbf{J} \cdot \mathbf{E}^*) \quad (4)$$

$$Q_{ml} = \frac{1}{2} \text{Re}(i\omega \mathbf{B} \cdot \mathbf{H}^*) \quad (5)$$

where Q_e is the electromagnetic power loss, Q_{rh} – the resistance loss, Q_{ml} – the magnetic loss, Re – the real part of the relative permittivity, i – the imaginary part, \mathbf{J} – the current density, \mathbf{B} – the magnetic flux density, and \mathbf{H} – the magnetic field strength.

Since the solid heat transfer equation is divided into frequency domain and transient state, we have [17]:

$$\rho C_p \mathbf{u} \nabla T + \nabla \mathbf{q} = Q_e + Q_{ted} \quad (6)$$

$$\rho C_p \frac{\partial T}{\partial t} + \rho C_p \mathbf{u} \nabla T + \nabla \mathbf{q} = Q_e + Q_{ted} \quad (7)$$

$$\mathbf{q} = -k \nabla T \quad (8)$$

where ρ is the material density, C_p – the constant pressure specific heat capacity, T – the absolute temperature, \mathbf{u} – the velocity vector of the average movement, \mathbf{q} – the conduction heat flux density, Q_{ted} – thermoelastic damping, and k – the thermal conductivity.

The resonant cavity and the boundary of the microwave feed port are made of copper-based materials. The rest of the space is filled with air except for the mineral model. The convective heat transfer coefficient between the material surface and air is set as 15 W/(m²K). The input power is 1000 W and 2000 W, respectively. The frequency is 2.45 GHz, and the irradiation time is 120 seconds. The specific parameters are shown in tab. 2, among them, the dielectric constant is measured by the dielectric constant measuring system composed of a vector network analyzer, waveguide coaxial converter and ridge waveguide at the Applied Electromagnetic Research Institute of Sichuan University.

Table 2. Material parameters [18-20]

Material	Density [kgm ⁻³]	Relative permeability	Conductivity [Sm ⁻¹]	Relative permittivity	Thermal conductivity [Wm ⁻¹ K ⁻¹]	Constant-pressure heat capacity [Jkg ⁻¹ K ⁻¹]
Air	–	1	0	1	–	–
Copper	–	1	5.998·10 ⁷	1	–	–
Quartz	2648	1	0	3.298 – 0.003958 <i>i</i>	<i>k</i> (<i>T</i>)	<i>C_p</i> (<i>T</i>)
Feldspar	2703	1	0	4.62 – 0.0231 <i>i</i>	1.46	<i>C_p</i> (<i>T</i>)
Dolomite	3795	1	0	6.56 – 0.012464 <i>i</i>	<i>k</i> (<i>T</i>)	<i>C_p</i> (<i>T</i>)

Study on the mechanism of electromagnetic thermal coupling in the microwave field

When the frequency is 2.45 GHz and the power is 1000 W, the temperature evolution rule of typical points is as shown in fig. 9. Generally, the temperature increases with the extension of the irradiation time. Figure 9(a) shows that Point 3, representing dolomite mineral, has the fastest internal temperature rise rate and the highest temperature (145.46 °C). Feldspar follows (109.19 °C), and quartz has the slowest temperature rise (95.41 °C). The evolution rule of the mineral temperature rise is consistent with the dielectric loss value of the mineral. Figures 9(b) and 9(c) represent the evolution diagram of the indirect contact temperature of the minerals. Point 4 represents the feldspar quartz contact point, with a maximum temperature of 96.69 °C in 120 seconds, Points 5 and 6 reach maximum temperatures of 124.85 °C and 144.83 °C, respectively, and the maximum temperature of Point 7 is 122.29 °C after 120 seconds. Figure 9 show that the temperature between the contact points of the minerals is between the maximum and minimum temperatures, but the gradients in the temperature reduction are different.

To further explore the relationship between the temperature distribution and electric field strength in the microwave field, the typical surface temperature distribution and electric field distribution are analyzed. As shown in fig. 10, the electric field, due to the disturbance of the dielectric material, is not evenly distributed under the absorption effect, showing a disordered state. Figure 11 shows that the temperature distribution of typical Plane 1 shows a decreasing

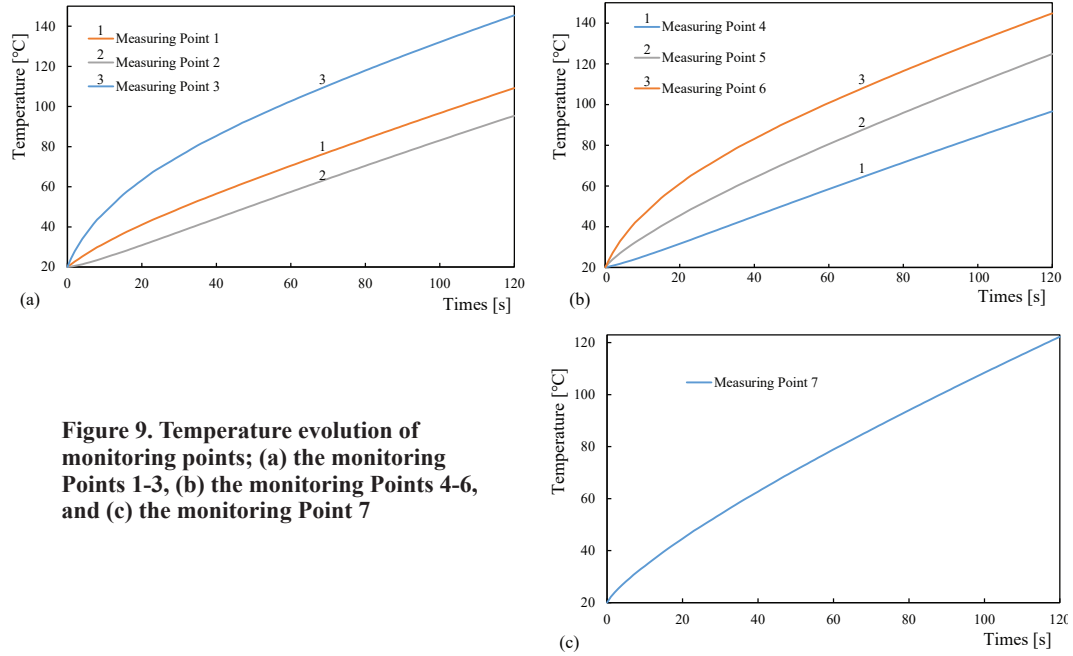


Figure 9. Temperature evolution of monitoring points; (a) the monitoring Points 1-3, (b) the monitoring Points 4-6, and (c) the monitoring Point 7

trend from the middle to both sides. The temperature distribution of typical Planes 2~4 is almost the same as that of the electric field intensity, showing a trend of high in the middle and low on both sides. It can be concluded from figs. 10 and 11 that the temperature distribution of dielectric materials is controlled mainly by the distribution of dielectric loss of the internal materials, and the distribution of the electric field can disturb the temperature distribution only slightly.

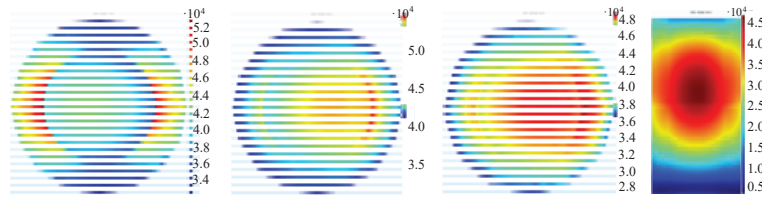


Figure 10. Electric field intensity distribution of typical Planes 1-4 (for color image see journal web site)

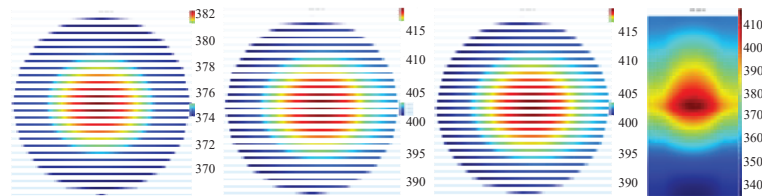


Figure 11. Temperature distribution of typical Surfaces 1-4

When the frequency is 2.45 GHz and the power is 2000 W, the temperature evolution rule of typical points is as shown in fig. 12. The general trend is the same as that of 1000 W. The

highest temperatures of dolomite, feldspar and quartz in the dielectric material are 1.86, 1.71, and 1.63 times the corresponding maximum temperature at 1000 W. According to eq. (1), the temperature scale factor of each component in the dielectric material under 2000 W and 1000 W irradiation is calculated. The calculation results, shown in fig. 13, indicate that the temperature scale factor reaches a stable state after the initial rise. The temperature scale factor of dolomite is stable between 1.7 and 1.8, while those of feldspar and quartz are stable at approximately 1.6-1.7 and 1.5-1.6, respectively.

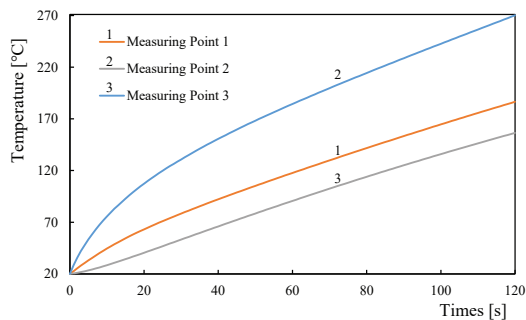


Figure 12. Temperature evolution of monitoring Points 1-3

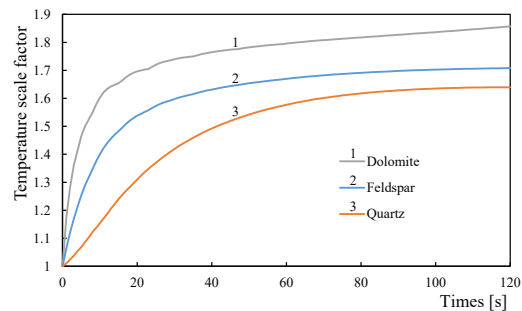


Figure 13. Temperature coefficient ratio of monitoring Points 1-3

Conclusion

According to the characteristics of electromagnetic heat generation of 1050 m deep sandstone and its minerals in a microwave field, the mechanism of electromagnetic heat generation in the microwave field was analyzed by means of the real-time indoor temperature monitoring tests and numerical simulations. There is asynchrony in the temperature rise between different areas in the same material. The rate of temperature rise depends on the dielectric properties of the region, and the maximum temperature that the temperature rise can reach depends on the local maximum heat storage capacity of the material. The heating rate of different minerals shows a trend of increasing first and then decreasing and the heating efficiency of different minerals does not increase with the increase of the power but is nevertheless affected by the characteristics of the minerals themselves. The temperature growth trend of the dielectric material decreases over time. The temperature growth and distribution are controlled mainly by the dielectric loss of the internal material, and the distribution of the electric field strength can disturb the temperature distribution only slightly. It is shown that the increase of temperature in microwave field is lower than that of microwave power, indicating that the thermal efficiency of microwave will decrease with the increase of power.

Acknowledgement

This work was financially supported by Sichuan International Technological innovation Cooperation Project (2018HH0159) and National Natural Science Foundation of China (51822403).

Nomenclature

B – magnetic flux density, [Wb m^{-3}]
 C_p – specific heat capacity, [$\text{J kg}^{-1} \text{K}^{-1}$]
E – electric field strength, [V m^{-1}]
H – magnetic field strength, [H m^{-1}]

i – imaginary part, [-]
J – current density, [A m^{-3}]
 k_0 – free space wave velocity, [ms^{-1}]
 k – thermal conductivity, [$\text{W m}^{-1} \text{K}^{-1}$]

Q_e – electromagnetic power loss, [Wm^{-3}]
 Q_{ml} – magnetic loss, [Wm^{-3}]
 Q_{rh} – resistance loss, [Wm^{-3}]
 Q_{ted} – thermoelastic damping, [Wm^{-3}]
 q – scale factor
 \mathbf{q} – conduction heat flux density, [Wm^{-2}]
 Re – real part of the relative permittivity, [–]
 T_p – temperature, [$^{\circ}\text{C}$]

T – absolute temperature, [K]
 \mathbf{u} – velocity vector, [ms^{-1}]

Greek symbols

ε_0 – vacuum dielectric constant, [Fm^{-1}]
 ε_r – dielectric constant, [–]
 ρ – material density, [kgm^{-3}]
 σ – conductivity, [Sm^{-1}]
 ω – angular frequency, [rads^{-1}]

References

- [1] Xie, H. P., Research Framework and Anticipated Results of Deep Rock Mechanics and Mining Theory (in Chinese), *Advanced Engineering Sciences*, 49 (2017), 2, pp. 1-16
- [2] Gao, M. Z., et al., The Location Optimum and Permeability-Enhancing Effect of a Low-Level Shield Rock Roadway, *Rock Mechanics & Rock Engineering*, 51 (2018), Apr., pp. 2935-2948
- [3] Rowson, N. A., Microwave Treatment of Minerals – A Review, *Minerals Engineering*, 11 (1998), 11, pp. 1081-1087
- [4] Niu, B., et al., Application of Pyrolysis to Recycling Organics from Waste Tantalum Capacitors, *Journal of Hazardous Materials*, 335 (2017), Aug., pp. 39-46
- [5] Jones, D.A., et al., Microwave Heating Applications in Environmental Engineering – A Review, *Resources Conservation & Recycling*, 34 (2002), 2, pp. 75-90
- [6] Kumar, R. C., et al., Microwave Assisted Extraction of Oil from Pongamia Pinnata Seeds, *Materials Today Proceedings*, 5 (2018), 1, pp. 2960-2964
- [7] Tassou, S. A., Quality Assurance in Microwave Food Processing and the Enabling Potentials of Solid-State Power Generators: A Review, *Journal of Food Engineering*, 234 (2018), Oct., pp. 1-15
- [8] Kingman, S. W., Rowson, N. A., Microwave Treatment of Minerals – A Review, *Minerals Engineering*, 11 (1998), 11, pp. 1081-1087
- [9] Olubambi, P. A., Influence of Microwave Pretreatment on the Bioleaching Behaviour of Low-Grade Complex Sulphide Ores, *Hydrometallurgy*, 95 (2009), 1-2, pp. 159-165
- [10] Olubambi, P. A., et al., Influence of Microwave Heating on the Processing and Dissolution Behaviour of Low-Grade Complex Sulphide Ores, *Hydrometallurgy*, 89 (2007), 1-2, pp. 127-135
- [11] Hassani, F., et al., The Influence of Microwave Irradiation on Rocks for Microwave-Assisted Underground Excavation, *Journal of Rock Mechanics and Geotechnical Engineering*, 8 (2016), 1, pp. 1-15
- [12] Lu, G. M., et al., Experimental Investigation on the Effects of Microwave Treatment on Basalt Heating, Mechanical Strength, and Fragmentation, *Rock Mechanics & Rock Engineering*, 52 (2019), 8, pp. 2535-2549
- [13] Gao, M. Z., et al., The Dynamic Failure Mechanism of Coal and Gas Outbursts and Response Mechanism of Support Structure, *Thermal Science*, 23 (2019), Suppl. 3, pp. S867-S875
- [14] Gao, M. Z., et al., Field Experiments on Fracture Evolution and Correlations Between Connectivity and Abutment Pressure under Top Coal Caving Conditions, *International Journal of Rock Mechanics and Mining Sciences*, 111 (2018), Nov., pp. 84-93
- [15] Pitchai, K., et al., A Microwave Heat Transfer Model for a Rotating Multi-Component Meal in a Domestic Oven: Development and Validation, *Journal of Food Engineering*, 128 (2014), May, pp. 60-71
- [16] Jiajia, C., et al., Heat and Mass Transport during Microwave Heating of Mashed Potato in Domestic Oven-Model Development, Validation, and Sensitivity Analysis, *Journal of Food Science*, 79 (2014), 10, pp. E1991-E2004
- [17] Li, J., et al., Fully-Coupled Simulations of Thermally-Induced Cracking in Pegmatite Due to Microwave Irradiation, *Journal of Rock Mechanics & Geotechnical Engineering*, 11 (2019), 2, pp. 242-250
- [18] Ali, A.Y., et al., Quantifying Damage around Grain Boundaries in Microwave Treated Ores, *Chemical Engineering & Processing*, 48 (2009), 11-12, pp. 1566-1573
- [19] Toifl, M., et al., 3D Numerical Study on Microwave Induced Stresses in Inhomogeneous Hard Rocks, *Minerals Engineering*, 90 (2016), May, pp. 29-42
- [20] Meisels, R., et al., Microwave Propagation and Absorption and Its Thermo-Mechanical Consequences in Heterogeneous Rocks, *International Journal of Mineral Processing*, 135 (2015), Feb., pp. 40-51

Paper submitted: August 3, 2019

Paper revised: January 10, 2020

Paper accepted: May 20, 2020

© 2020 Society of Thermal Engineers of Serbia

Published by the Vinča Institute of Nuclear Sciences, Belgrade, Serbia.

This is an open access article distributed under the CC BY-NC-ND 4.0 terms and conditions